



Original Article

Are the CTV-to-PTV margins currently used in online adaptive radiotherapy for prostate cancer too large? The impact of the distribution of microscopic disease on treatment margin requirements

Mathijs G. Dassen^{a,1}, Marcel van Herk^b, Marnix G. Witte^a, Tomas Janssen^a, Floris Pos^a,
Uulke A. van der Heide^{a,*}

^a Department of Radiation Oncology, The Netherlands Cancer Institute, Amsterdam, the Netherlands

^b Department of Radiation Oncology, The Christie NHS Foundation Trust, Manchester, United Kingdom



ARTICLE INFO

Keywords:

Prostate cancer
Margins
Microscopic disease
Intra-fraction motion
Online adaptive radiotherapy

ABSTRACT

Purpose: Planning target volume (PTV) margin recipes assume all parts of the target are equally important. For the prostate clinical target volume (CTV) this is invalid. We evaluated the impact of the spatial probability distribution of microscopic disease in the prostate on CTV-to-PTV margins.

Materials and methods: A prostate with a volume of 44 cm³ was defined as CTV_{prostate}. Homogenous dose distributions were created with margins ranging 0–5 mm. The gross tumor volume (GTV) was assumed covered with a separate margin. Microscopic satellites were sampled within the CTV_{prostate} from a histopathology-based probability distribution for a range of numbers (1–10) and sizes (0.02–0.2 cm³) to define CTV_{satellites}. Geometric errors were sampled from a 3D Gaussian distribution, simulating online adaptive treatment of 5 fractions. Each CTV was shifted with respect to the dose according to each total error. The PTV margin ensuring 95 % of the prescribed dose to the CTV_{satellites} in 90 % of simulations was determined and compared with CTV_{prostate}.

Results: For systematic errors with width (Σ) 0.5 mm and random errors with width (σ_r) 1.5 mm, the margin for the CTV_{prostate} was 3 mm, whereas for each definition of CTV_{satellites} this margin was 0–1 mm. For $\sigma_r = 2.7$ mm, a margin of 5 mm was adequate for the CTV_{prostate} and 2–3 mm for all except the most favourable and unfavourable CTV_{satellites} definition.

Conclusion: The CTV-to-PTV margins used in online adaptive radiotherapy for prostate cancer can be reduced by ~2 mm, if the GTV is covered with an adequate margin.

Introduction

Radiotherapy aims to deliver a curative dose to the tumor cells while minimizing the dose to healthy tissue. To this end, the gross tumor volume (GTV) and clinical target volume (CTV) are delineated prior to treatment planning. The accuracy of dose delivery is limited by geometric uncertainties, including for example inter- and intrafraction motion. To ensure adequate coverage of a target volume, ICRU report 50 defined a planning target volume (PTV) [1]. PTV margin recipes aim to guarantee coverage of a specified dose in the population. Most commonly, a margin is designed such that 90 % of the patients receive a minimum of 95 % of the prescribed dose to the CTV [2]. These recipes assume that all parts of the target are equally important. This implies that any

geometrical miss of the CTV is expected to result in underdosing some tumor cells. In particular for the CTV, designed to cover microscopic disease, pathological evidence indicates that this assumption does not hold. For example in breast, head-and-neck and lung cancer, the density of microscopic disease gradually decays with increasing distance from the GTV [3–5]. Stroom et al. proposed to incorporate this decay in cell density in the margin recipe for defining a GTV-to-PTV margin [6].

Prostate cancer is predominantly a multifocal disease consisting of one or more satellite lesions next to the largest (index) lesion [7–11]. The majority of these satellite lesions have a volume of <0.1 cm³ and is therefore likely not visible on diagnostic imaging [12,13]. Consequently, they are not included in the GTV, which holds approximately 95–98 % of the total tumor load [10,11]. The location and genomic

* Corresponding author at: Department of Radiation Oncology, The Netherlands Cancer Institute, Plesmanlaan 121, 1066 CX Amsterdam, the Netherlands.

E-mail addresses: t.dassen@nki.nl (M.G. Dassen), u.vd.heide@nki.nl (U.A. van der Heide).

¹ First author: Department of Radiation Oncology, The Netherlands Cancer Institute, Plesmanlaan 121, 1066 CX Amsterdam, The Netherlands.

profile of these microscopic satellites in the prostate appears uncorrelated with that of the GTV [10,14]. Therefore, in clinical practice the whole prostate gland is included as CTV. However, since microscopic disease is not homogeneously distributed, it is possible that a geometrical miss of the CTV will not result in underdosing any tumor cells because this part may hold no tumor cells at all. We hypothesize that by explicitly considering the distribution of microscopic disease in the prostate, the PTV margin can be reduced while ensuring that the tumor cells receive a minimum of 95 % of the prescribed dose in 90 % of the patients. Hence, this could improve the balance between target coverage and dose exposure to organs at risk surrounding the prostate. Importantly, this reasoning does not apply to the GTV. Because this holds macroscopically visible tumor any underdosage of this volume would undertreat some of the tumor cells. Therefore conventional margin recipes should be applied for the GTV.

Here we investigate the implications of the spatial distribution of microscopic disease in the prostate gland for the PTV margin applied to the CTV. We explicitly assume that the GTV is adequately covered with a separate PTV margin. We conducted a series of Monte Carlo simulations, simulating a distribution of tumor satellites with varying size and number, using the tumor prevalence map developed by Ou et al. [15–17]. We simulated a range of geometrical errors that can be expected in modern online adaptive radiotherapy. We calculated the dose coverage of the satellites and the PTV margins required to guarantee a predefined coverage criterion.

Materials and methods

We studied the implications of the spatial distribution of microscopic disease in the prostate for PTV margins for the CTV in a modern online adaptive treatment setting. We considered treatment of a homogeneous dose planned to be delivered to the CTV in 5 fractions. The GTV including any surrounding microscopic spread directly attached to the GTV was assumed to be covered using a separate GTV-to-PTV margin.

Sampling of satellites to model microscopic disease

The tumor prevalence map of Ou et al. was constructed out of 158 prostatectomy specimen and consists of the spatial probability of finding tumor cells in a population averaged prostate [15,16]. Each voxel in this map represents the fraction of specimen that showed tumor cells at that location. In the original work the map was smoothed with an isotropic Gaussian filter. In addition, in later work by Dinh et al. the map was made symmetric in the left – right direction [17]. Both post-processing operations potentially induce a bias in the probability of finding tumor cells near the edge of the prostate. To remove this bias, in our experiments the prostate was cropped by 1 mm to define a boundary region and all voxels within this boundary volume kept the same value. We considered this tumor atlas to be our prostate CTV, having a volume of 44 cm³.

Next, we performed simulations to sample satellite locations within the prostate CTV. For this, the tumor prevalence map was converted into a point cloud of 100,000 points in which the point density corresponded to the probability of tumor cell presence in the map. In each simulation a random point was sampled from this point cloud and defined as the center of a spherical lesion, consisting of 100 points equally distributed over the total volume of the lesion. This resulted in a CTV_{satellites} consisting of one or multiple spherical lesions within the prostate CTV. To avoid overlap between lesions, all points from the tumor prevalence point cloud that were located within a distance of 2 times the radius of the lesion from the sampled point were removed before the next random sample. In addition, we did not allow lesions to extend outside the prostate CTV. In case a lesion was sampled at the edge of the CTV, the fraction of points of the lesion that extended the CTV was removed. The CTV_{prostate} used as reference in the study, consisted of the prostate CTV and was defined by 100,000 points equally divided over the total

volume.

Geometric error distributions

The Van Herk margin recipe assumes an undeformable target volume and treatment uncertainties divided into preparation (systematic, Σ) and execution (random, σ_r) errors. These are assumed to be normally distributed and independent and are derived from population statistics. The distributions of Σ and σ_r used in our simulations were obtained from a 3D Gaussian random number generator. We determined the width of Σ and σ_r to approximate the PTV margins currently used for the prostate, ranging from 3 mm in an MRI-guided online workflow to 5 mm in an CBCT-guided online workflow [18–20]. In daily online adaptation the systematic error is minimized, however a residual error will always be present as a result of uncertainties related to the treatment machine, such as gantry positioning and MLC motion [21,22]. Therefore, the width of Σ was estimated to be 0.5 mm. Delineation uncertainties were excluded from the systematic error. Next, we used the Van Herk margin recipe to derive the width of σ_r . We simulated a treatment to be delivered in 5 treatment fractions (N). Then, σ_r results in both a random (σ_{eff}) and a systematic error component adding to the total systematic error (Σ_{eff}) [23–25]:

$$\sigma_{eff}^2 = \frac{N-1}{N} \sigma_r^2$$

$$\Sigma_{eff}^2 = \Sigma^2 + \frac{1}{N} \sigma_r^2$$

By accounting for the finite number of fractions the width of σ_r was 1.5 mm and 2.7 mm resulting in a Σ_{eff} of 0.8 mm and 1.3 mm and a σ_{eff} of 1.3 mm and 2.4 mm to approximate a PTV margin of 3 mm and 5 mm, respectively. In addition, we evaluated the potential added value of beam-gated radiotherapy in case of using a gating window of 2 mm. For this, we adjusted σ_r by discarding all displacement vectors larger than 2 mm in any direction before sampling random errors.

Dose distributions

We created PTV-based homogenous dose distributions convolved with Gaussian penumbra (σ_p) of width 3.2 mm on a 1 mm resolution cubic grid. For this, we assumed the prostate CTV as target volume with PTV margins ranging 0–5 mm in steps of 1 mm. Similar to clinical practice, each voxel included in the PTV received at least 95 % of the prescribed dose [26]. In contrast to the Van Herk recipe, in which a spherical target and a perfectly conformal dose distribution is assumed, the prostate CTV is not perfectly spherical. Consequently, the dose distributions used in our experiments showed non-perfect conformity to the PTV. As a control experiment, we repeated our simulations using idealized dose distributions based on a perfect sphere with the same volume as the prostate CTV (CTV_{sphere}).

Experiments

A schematic overview of the experiments is shown in Fig. 1. First, Monte Carlo simulations were used to sample satellite distributions from the tumor prevalence map. We performed simulations across a range of number (1–10) and size (0.02–0.2 cm³) of satellites. These ranges were based on data from prostatectomy specimens [10,11]. For each potential combination of number and size of satellites 1000 simulations of the CTV_{satellites} were performed. Next, Monte Carlo simulations were also used to sample errors from the geometric error distributions [27,28]. For this, we sampled 5000 systematic errors and for each systematic error 5 daily random errors were sampled and consecutively added. Each CTV_{satellites} was then shifted with respect to the dose distribution according to each total error. We evaluated the minimum dose delivered to the CTV_{satellites} in 90 % of all combinations of CTV_{microscopic} and total

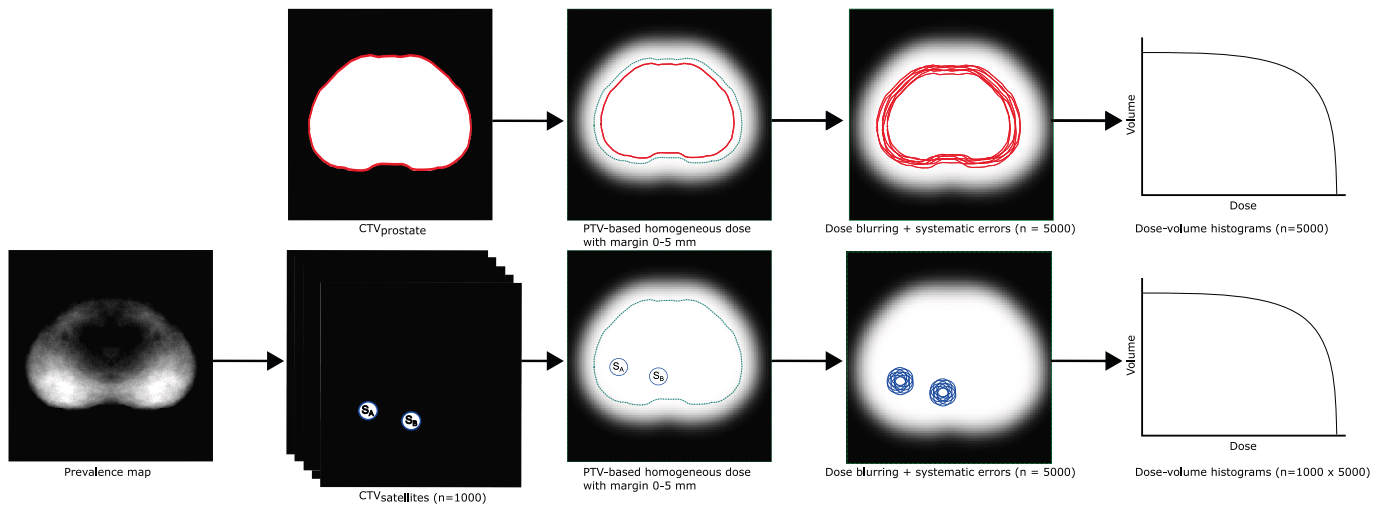


Fig. 1. Schematic overview of the experiments. Satellites were sampled from a tumor prevalence map for a range of number (1–10) and size (0.02–0.2 cm³) to model potential distributions of microscopic disease in the prostate (CTV_{satellites}). For each combination of number and size 1000 samples were performed. The CTV_{prostate} consisted of the total volume of prostate. Next, PTV-based homogeneous dose distributions were created with PTV margins ranging 0–5 mm. Geometric errors expected in online adaptive radiotherapy delivered in 5 fractions were simulated by sampling random and systematic errors (n = 5000). We evaluated the minimum dose delivered to the CTV in 90 % of the population of simulations.

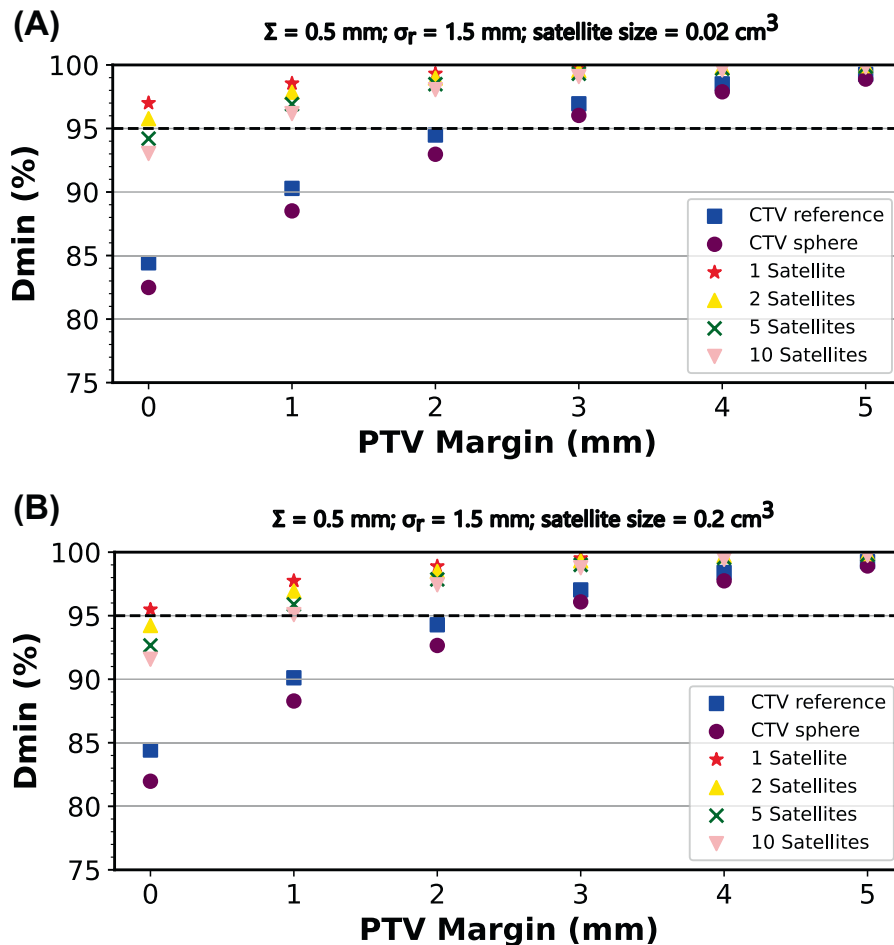


Fig. 2. Coverage of the CTV_{prostate}, CTV_{sphere} and different definitions of the CTV_{satellites} for margins up to 5 mm, in case of simulating geometric errors with $\Sigma = 0.5$ mm and $\sigma_r = 1.5$ mm. Satellites lesion were simulated with a size ranging (A) 0.02 cm³ to (B) 0.2 cm³. Each dot represents the Dmin as a percentage of the prescribed dose that was delivered to each CTV in 90 % of the simulations. The horizontal dashed line corresponds with the coverage criterion used to determine the appropriate PTV margin.

errors ($n = 5,000,000$). Similarly, the $CTV_{prostate}$ and CTV_{sphere} were shifted with respect to their corresponding dose distribution. In this case, we evaluated the minimum dose delivered to the $CTV_{prostate}$ and CTV_{sphere} in 90 % of the total errors ($n = 5000$). Finally, we determined the PTV margin for which the criterion of receiving at least 95 % of the prescribed dose to the CTV in 90 % of the population of simulations was fulfilled and compared these for each of the defined CTVs.

Results

For geometric errors of $\Sigma = 0.5$ mm and $\sigma_r = 1.5$ mm a minimum dose of 95 % of the prescribed dose in 90 % of the population of simulations was reached for a PTV margin of 3 mm for the $CTV_{prostate}$ (Fig. 2A and B) consistent with the predefined widths of the systematic and random error distributions. For the CTV_{sphere} , we found the same result. For each distribution of satellites, the $CTV_{satellites}$ coverage was >99 % in 90 % of the simulations for this same PTV margin. A PTV margin of 1 mm would already be sufficient to fulfill the coverage criterion of >95 % of the prescribed dose in 90 % of the simulations. For the more favourable definitions of $CTV_{satellites}$, consisting of 1–2 satellites with a size of 0.02 cm³ or 1 satellite with a size of 0.2 cm³, a PTV margin of 0 mm sufficed. We further observed that the differences in minimum dose coverage in 90 % of the simulations between all simulated definitions of $CTV_{satellites}$, varying in size and number, were small relative to the difference in coverage with the $CTV_{prostate}$.

We found similar results for the experiments simulating geometric

errors expected in to result in a PTV margin of 5 mm (Fig. 3A and B). The PTV margin required for the $CTV_{prostate}$ also matched with the predefined geometric errors distributions. For the CTV_{sphere} , a minimum dose of 94 % of the prescribed dose was delivered in 90 % of the simulations for the same PTV margin. For the $CTV_{satellites}$, a reduced PTV margin of 3 mm would be appropriate for each of the simulated distributions, except for the most unfavourable definition of the $CTV_{satellites}$ consisting of 10 satellite lesions with a size of 0.2 cm³. For the more favourable definitions of $CTV_{satellites}$, again consisting of 1–2 satellites with a size of 0.02 cm³ or 1 satellite with a size of 0.2 cm³, a PTV margin of 2 mm was appropriate.

The simulations of beam-gated radiotherapy, using a gating window of 2 mm, showed that a 0 mm PTV margin would be sufficient to ensure adequate coverage to each $CTV_{satellites}$, except for the most unfavorable definition of the $CTV_{satellites}$ (Fig. 4A and B). For this extreme case, the minimum dose in 90 % of the simulations was 94 % of the prescribed dose.

Discussion

The aim of this study was to evaluate the impact of the spatial distribution of tumor cells in the prostate outside the GTV on the required PTV margins for the CTV. Our results show that with geometric uncertainties achievable in online adaptive radiotherapy, the PTV margin can be reduced by approximately 2 mm compared to the typical margins used in clinical practice of 3–5 mm. For the specific case of beam-gated

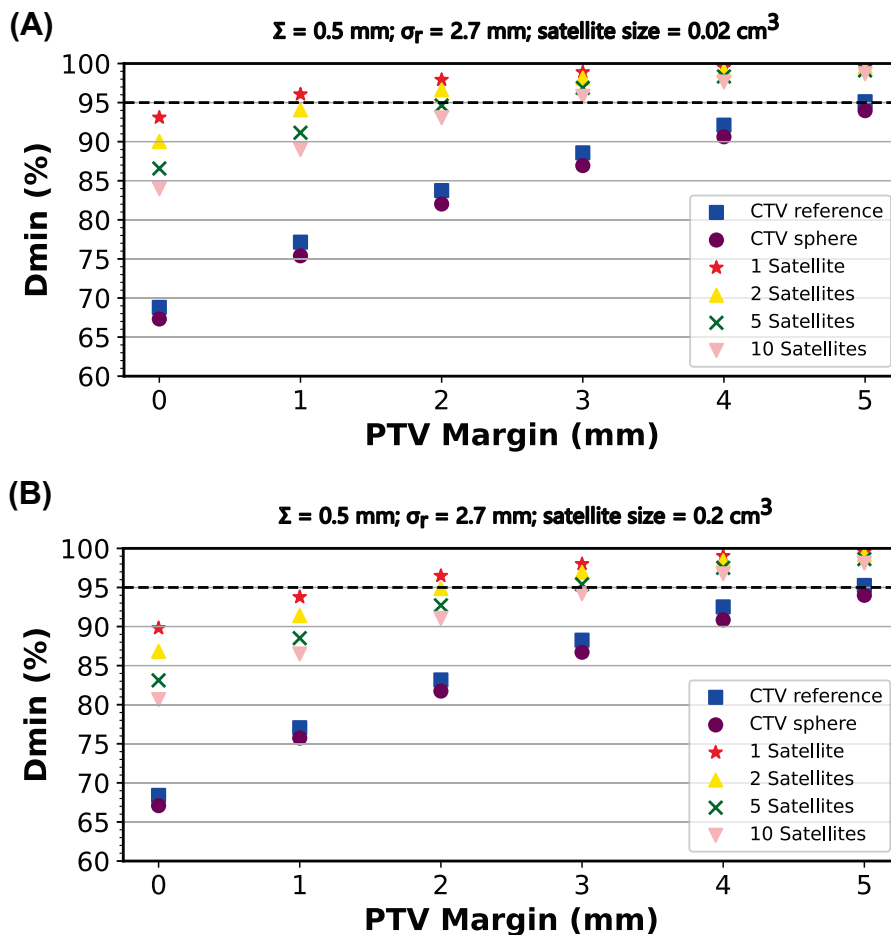


Fig. 3. Coverage of the $CTV_{prostate}$, CTV_{sphere} and different definitions of the $CTV_{satellites}$ for margins up to 5 mm, in case of simulating geometric errors with $\Sigma = 0.5$ mm and $\sigma_r = 2.7$ mm. Satellite lesions were simulated with a size ranging (A) 0.02 cm³ to (B) 0.2 cm³. Each dot represents the Dmin as a percentage of the prescribed dose that was delivered to each CTV in 90 % of the simulations. The horizontal dashed line corresponds with the coverage criterion used to determine the appropriate PTV margin.

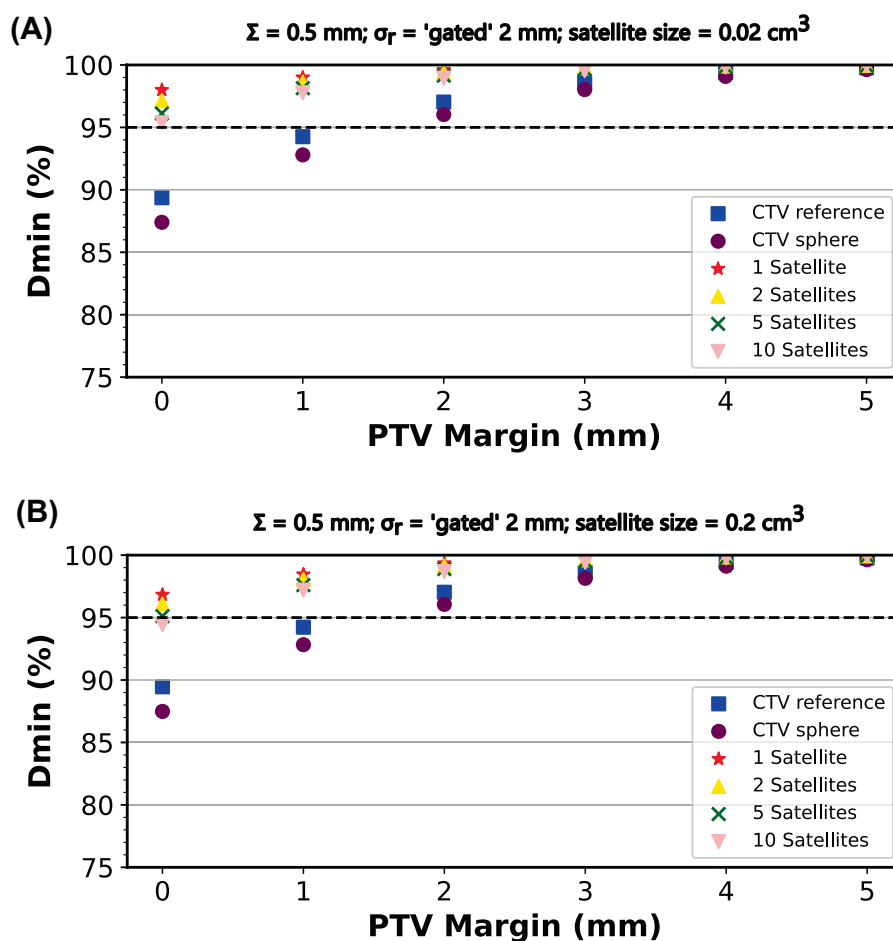


Fig. 4. Coverage of the CTV_{prostate}, CTV_{sphere} and different definitions of the CTV_{satellites} for margins up to 5 mm, in case of simulating geometric errors expected in beam-gated radiotherapy using a gating window of 2 mm. Satellites lesion were simulated with a size ranging (A) 0.02 cm³ to (B) 0.2 cm³. Each dot represents the Dmin as a percentage of the prescribed dose that was delivered to each CTV in 90 % of the simulations. The horizontal dashed line corresponds with the coverage criterion used to determine the appropriate PTV margin.

radiotherapy using a gating window of 2 mm around the CTV, all tumor cells in the CTV may be covered adequately using a 0 mm PTV margin.

In online adaptive radiotherapy, where treatment preparation is performed every fraction just prior to irradiation, random treatment execution errors dominate over systematic treatment preparation errors. These random errors result in a dose blurring that has limited impact on target coverage in case these errors are smaller than the dose penumbra [2]. For the prostate as target volume these conditions are fulfilled and consequently the PTV margins used in clinical practice are small, ranging 3–5 mm [17–19]. Our simulations of geometric errors were based on a heuristic approach, defining a residual set-up error ($\Sigma = 0.5$ mm) and then determining a range of σ_r (1.5–2.7 mm) to approximate the range of clinical margins. While Σ is inherently machine-specific, variations are typically within submillimeter ranges [21,22]. The range of σ_r is assumed to be a reasonable approximation, as the expected intra-fraction motion ranges 0–5 mm [29] and interobserver variability for contouring the prostate CTV is approximately 1 mm, with CBCT showing larger variability compared to MRI [30]. In addition, the underlying principle that drives our results is that the probability of tumor cell presence at the edge of the CTV is small relative to the probability that this part of the CTV will not receive the prescribed dose. Therefore, our results are expected to be generalizable to other potential combinations of Σ and σ_r that correspond to the same range of clinical margins. Note that our simulations are purely geometrical and are not based on tumor control probability (TCP) modeling. It could be that inclusion of TCP calculation further reduces margin requirements as shown in van

Herk et al. [27].

We assume that the GTV is covered adequately using a separate GTV-to-PTV margin, which requires careful consideration and is not guaranteed without appropriate imaging. With multiparametric MRI (mp-MRI), tumor volume tends to be underestimated as demonstrated by histopathology-matched studies [31–34] and substantial interobserver variability, particularly intra-prostatically, has been reported [35]. Regions with characteristics corresponding to lower risk disease are more likely to be missed in the delineation of GTV [32]. Reported margins, required to improve agreement between MRI and histopathology, vary widely in literature (range 1–9 mm) [31,33]. The addition of PSMA-PET to mp-MRI may help to improve the accuracy of GTV definition [34,36]. The FLAME trial, on the other hand, achieved excellent outcomes by applying a focal boost without any margins applied to the GTV [37]. Altogether, these considerations emphasize that adequate coverage of the GTV depends on a balance between delivered dose and the chosen CTV and PTV margins and this interplay should not be oversimplified.

A limitation of our simulations of geometric errors is the assumption that these errors are random, isotropic and do not include any rotations or deformations. Especially intra-fraction motion of the prostate, influenced by both bladder and rectal filling, is known to be most present over the anterior-posterior and cranial-caudal axis and may include substantial rotations [38]. However, this assumption is in line with the assumption in the Van Herk margin recipe. Since we are excluding the GTV in our simulations rotations of the semi-spherical CTV likely has small impact [39]. Importantly, any small underestimation due to

excluding rotations would likely affect the margins for both the CTV and microscopic disease similarly, and our control experiment confirmed that conventional margins could be reproduced under these assumptions. In addition, our control experiment also showed that the impact of a non-perfect conformality based on a realistic prostate shape was small and did not significantly impact our analysis. Furthermore, we did not use dose distributions from clinical treatment plans. Instead, we applied a gradient estimate ($\sigma_p = 3.2$ mm) that represents a relatively steep dose fall-off and reflects a conservative worst-case scenario. Another limitation is that we used one average CTV size (44 cm^3) in our simulations. We acknowledge there is an interplay between the CTV size and the size of a microscopic lesion on the likelihood of occurrence near the CTV boundary. However, we argue that we addressed this effect by simulating a wide range of lesion sizes and numbers. Given that PTV margins are based on population statistics we also believe that the use of an average-sized prostate provides a reasonable estimate.

We simulated beam-gated radiotherapy using a gating window of 2 mm because intra-fraction motion of the prostate is typically <3 mm [29], consistent with $\sigma_r = 1.5$ mm. In order to decrease the effective intra-fraction motion, justifying a reduction of the PTV margin, the gating window should be smaller than the motion expected during treatment delivery [40,41]. However, intra-fraction motion of >5 mm may appear in a small proportion of patients, consistent with $\sigma_r = 2.7$ mm. In this case the gating duty cycle will become <80 % for a gating window of 2 mm, which may have clinical implications for the risk of toxicity [42]. In addition, motion mitigation via gating is currently based on 2D cine MRI acquisitions for which a tracking mismatch with the 3D reference image may occur between anatomical planes [43], which we did not take into account in our simulations.

Our simulations of microscopic disease were based on histopathological data supporting the assumption that the GTV constitutes approximately 95–98 % of the total tumor load. Consequently, we assumed that 2–5 % of the tumor load consist of microscopic disease, distributed over a number of satellite lesions [10,11]. To test the impact of this assumption, simulations were performed over a range of scenario's, from very favourable (microscopic disease consisting of 1 satellite lesion with a small size) to very unfavourable (10 satellite lesions with a size that is likely visible on diagnostic imaging [12,13]). These ranges correspond to a total volume of 0.02 – 2 cm^3 and given that the GTV most commonly encompasses 0.5 – 8 cm^3 [33,44,], we argue that our simulations sufficiently reflect the potential tumor load of microscopic disease. Moreover, the most realistic scenario is considered to lie somewhere between these extremes [45–47] and our results showed that the differences in coverage for all potential definitions of the CTV_{satellites} were relatively small.

We assumed that all microscopic spread was included in the prostate CTV and therefore we did not allow sampled satellite lesions to extend outside this volume. For this, we discarded the points of the lesion extending outside the prostate CTV. The resulting volume reduction of some lesions does not impact our analysis because the coverage criterion is based on accumulated minimum dose, which will always be located at the CTV surface. The assumption is consistent with the ESTRO guideline on target delineation for prostate cancer, which recommends extending the CTV beyond the capsule in case of suspected microscopic disease beyond the capsule [48]. Extraprostatic extensions (EPE) are most commonly localized in connection with the GTV and can therefore be covered by applying a 3 mm margin to the GTV, extending the CTV. We acknowledge that in rare cases EPE may also occur at a location distant from the GTV, although conclusive data on the frequency and distribution of these cases is currently not available. We argue that their potential impact has been addressed in our study through inclusion of delineation uncertainty within the modeled range of geometrical errors used in our simulations.

Local recurrences currently predominantly occur at the location of the original GTV rather than at the edge of the CTV at a location way from the GTV [49]. Nevertheless, we acknowledge that reducing the

CTV-to-PTV margin without a corresponding reduction of geometric uncertainties has the theoretical risk of increasing the number of recurrences at locations of microscopic disease near the edge of the CTV. The DESTINATION-MRL (NCT06284304) and DESTINATION 2 (NCT06638541) trials are the first prospective trials testing the use of a 0 mm CTV-to-PTV margin in online adaptive MRI-guided radiotherapy, with DESTINATION 2 additionally employing a gating strategy.

The impact of microscopic disease spread within the CTV on treatment margins has been studied before. Stroom et al., proposed a margin recipe based on a gradual decay in cell density away from the GTV as observed in breast and lung tumors [3]. By directly constructing a GTV-to-PTV margin, instead of first constructing a CTV, the total margin could be reduced for these tumor sites. In the prostate, however, microscopic spread does not show a distance relation to the GTV and therefore this margin recipe will not be applicable. Susharina et al. have introduced the clinical target distribution (CTD) which deals with CTV uncertainties by defining it as a continuous probability distribution of tumor cell presence from the boundary of the GTV [50]. Using the CTD instead of the CTV allows for a robust dose optimization process, in which coverage of the CTD is evaluated over a range of potential geometric errors to determine the optimal dose distribution [51]. These ideas were applied in focal boosting radiotherapy for prostate cancer, in which the aim was to escalate the dose to subregions in the prostate with probability of tumor presence based on a spatial probability map derived from mp-MRI [52]. However, since this spatial probability map was based on diagnostic imaging, microscopic spread of disease could not be captured accurately.

Our approach could potentially be applied to other tumor sites in which there is no clear distance relation between microscopic spread and to the primary tumor. For example, in patients with rectal cancer the whole mesorectum is generally considered to be included in the CTV. However, the risk of microscopic disease presence in the outer region of the mesorectum may be limited and appears uncorrelated with the location of the GTV [53].

Our experiments were based on accumulated minimum dose and did not incorporate an evaluation of TCP. Although a dose–effect relation was previously established for the GTV using a conventional treatment schedule of 35 fractions [54], currently insufficient data is available to translate this data into a dose–effect relation for microscopic disease using hypofractionated treatment schedules. We chose not to use TCP models because such an evaluation requires additional assumptions on histopathologic features of microscopic lesions, such as cell density and morphology [11].

In conclusion, this study showed that the CTV-to-PTV margins used in online adaptive radiotherapy for prostate cancer can be reduced by approximately 2 mm, as long as the GTV is covered with a separate GTV-to-PTV margin. This could potentially reduce the risk of toxicity by decreasing the dose delivered to healthy structures surrounding the prostate, while covering microscopic disease in the prostate adequately.

CRedit authorship contribution statement

Mathijs G. Dassen: Conceptualization, Methodology, Software, Investigation, Formal Analysis, Writing – Original Draft, Visualization. **Marcel van Herk:** Conceptualization, Methodology, Writing – Review & Editing. **Marnix G. Witte:** Methodology, Software, Writing – Review & Editing. **Tomas Janssen:** Conceptualization, Methodology, Writing – Review & Editing. **Floris Pos:** Conceptualization, Writing – Review & Editing. **Uulke A. van der Heide:** Conceptualization, Methodology, Writing – Review & Editing, Supervision.

Declaration of competing interest

All authors declare to have no known competing financial interests or personal relationships that could have appeared to influence the work reported in this paper.

References

- [1] ICRU report 50: Prescribing, recording and reporting photon beam therapy. Journal of the ICRU, 1993. Os-26. <https://doi.org/10.1093/jicru/os26.1.v>.
- [2] Van Herk M, Remeijer P, Rasch C, et al. The probability of correct target dosage: dose-population histograms for deriving treatment margins in radiotherapy. *Int J Radiat Oncol Biol Phys* 2000;47:1121–35. [https://doi.org/10.1016/S0360-3016\(00\)00518-6](https://doi.org/10.1016/S0360-3016(00)00518-6).
- [3] Stroom J, Blaauwgeers H, Van Baardwijk A, et al. Feasibility of pathology-correlated lung imaging for accurate target definition of lung tumors. *Int J Radiat Oncol Biol Phys* 2007;69:267–75. <https://doi.org/10.1016/j.ijrobp.2007.04.065>.
- [4] Stroom J, Schlieff A, Alderliesten T, et al. Using histopathology breast cancer data to reduce clinical target volume margins at radiotherapy. *Int J Radiat Oncol Biol Phys* 2009;74:898–905. <https://doi.org/10.1016/j.ijrobp.2009.01.026>.
- [5] Campbell S, Poon I, Markel D, et al. Evaluation of microscopic disease in oral tongue cancer using whole-mount histopathologic techniques: implications for the management of head-and-neck cancers. *Int J Radiat Oncol Biol Phys* 2012;82:574–81. <https://doi.org/10.1016/j.ijrobp.2010.09.038>.
- [6] Stroom J, Gilhuijs K, Vieira S, et al. Combined recipe for clinical target volume and planning target volume margins. *Int J Radiat Oncol Biol Phys* 2014;88:708–14. <https://doi.org/10.1016/j.ijrobp.2013.08.028>.
- [7] Chen ME, Johnston DA, Tang K, et al. Detailed mapping of prostate carcinoma foci: biopsy strategy implications. *Cancer* 2000;89:1800–9.
- [8] Wise AM, Stamey TA, McNeal JE, et al. Morphologic and clinical significance of multifocal prostate cancers in radical prostatectomy specimens. *Urology* 2002;60:264–9. [https://doi.org/10.1016/S0090-4295\(02\)01728-4](https://doi.org/10.1016/S0090-4295(02)01728-4).
- [9] Mouraviev V, Mayes JM, Sun L, et al. Prostate cancer laterality as a rationale of focal ablative therapy for the treatment of clinically localized prostate cancer. *Cancer* 2007;110:906–10. <https://doi.org/10.1002/ncr.22858>.
- [10] Hollmann BG, Van Triest B, Ghobadi G, et al. Gross tumor volume and clinical target volume in prostate cancer: how do satellites relate to the index lesion. *Radiother Oncol* 2015;115:96–100. <https://doi.org/10.1016/j.radonc.2015.01.021>.
- [11] Ghobadi G, De Jong J, Hollmann BG, et al. Histopathology-derived modeling of prostate cancer tumor control probability: Implications for the dose to the tumor and the gland. *Radiother Oncol* 2016;119:97–103. <https://doi.org/10.1016/j.radonc.2016.02.015>.
- [12] Van Houdt PJ, Ghobadi G, Schoots IG, et al. Histopathological features of MRI-invisible regions of prostate cancer lesions. *J Magn Reson Imag* 2020;51:1235–46. <https://doi.org/10.1002/jmri.26933>.
- [13] Gibbons M, Simko JP, Carroll PR, et al. Prostate cancer lesion detection, volume quantification and high-grade cancer differentiation using cancer risk maps derived from multiparametric MRI with histopathology as the reference standard. *Magn Reson Imag* 2023;99:48–57. <https://doi.org/10.1016/j.mri.2023.01.006>.
- [14] Haffner MC, Zwart W, Roudier MP, et al. Genomic and phenotypic heterogeneity in prostate cancer. *Nat Rev Urol* 2020;18:79–92. <https://doi.org/10.1038/s41585-020-00400-w>.
- [15] Shen D, Lao Z, Zeng J, et al. Optimized prostate biopsy via a statistical atlas of cancer spatial distribution. *Med Image Anal* 2004;139–50. <https://doi.org/10.1016/j.media.2003.11.002>.
- [16] Ou Y, Shen D, Zeng J, et al. Sampling the spatial patterns of cancer: Optimized biopsy procedures for estimating prostate cancer volume and Gleason score. *Med Image Anal* 2009;609–20. <https://doi.org/10.1016/j.media.2009.05.002>.
- [17] Dinh CV, Steenbergen P, Ghobadi G, et al. Multicenter validation of prostate tumor localization using multiparametric MRI and prior knowledge. *Med Phys* 2017;44:949–61. <https://doi.org/10.1002/mp.12086>.
- [18] Ariyaratne H, Chesham H, Pettingell J, et al. Image-guided radiotherapy for prostate cancer with cone-beam CT: dosimetric effects of imaging frequency and PTV margin. *Radiother Oncol* 2016;121:103–8. <https://doi.org/10.1016/j.radonc.2016.07.018>.
- [19] Byrne M, Teh AY, Achibald-Heeren B, et al. Intrafraction motion and margin assessment for ethos online adaptive radiotherapy treatments of the prostate and seminal vesicles. *Adv Radiat Oncol* 2023;9. <https://doi.org/10.1016/j.adro.2023.101405>.
- [20] Kusters J, Monshouwer R, Koopmans P, et al. Prostate motion in magnetic resonance imaging-guided radiotherapy and its impact on margins. *Strahlenther Onkol* 2025. <https://doi.org/10.1007/s00066-024-02346-z>.
- [21] van de Schoot AJ, Hoffmans D, van Ingen KM, et al. Characterization of Ethos therapy systems for adaptive radiation therapy: a multi-machine comparison. *J Appl Clin Med Phys* 2023;24. <https://doi.org/10.1002/acm2.13905>.
- [22] Bassiri N, Bayouth JE, Mittauer KE. Characterization of mechanical and radiation isocenter on an MR-guided radiotherapy (MRgRT) Linac. *J Appl Clin Med Phys* 2023;24. <https://doi.org/10.1002/acm2.14111>.
- [23] De Boer HCJ, Heijmen BJM. A protocol for the reduction of systematic patient setup errors with minimal portal imaging workload. *Int J Radiat Oncol Biol Phys* 2001;50:1350–65. [https://doi.org/10.1016/S0360-3016\(01\)01624-8](https://doi.org/10.1016/S0360-3016(01)01624-8).
- [24] Gorden JJ, Siebers JV. Convolution method and CTV-to-PTV margins for finite fractions and small systematic errors. *Phys Med Biol* 2007;52:1967–90. <https://doi.org/10.1088/0031-9155/52/7/013>.
- [25] Herschtal A, Foroudi F, Silva L, et al. Calculating geometrical margins for hypofractionated radiotherapy. *Phys Med Biol* 2013;58:319–33. <https://doi.org/10.1088/0031-9155/58/2/319>.
- [26] Eaton DJ, Naismith OF, Henry AM. Need for consensus when prescribing stereotactic body radiation therapy for prostate cancer. *Int J Radiat Oncol Biol Phys* 2015;91:239–41. <https://doi.org/10.1016/j.ijrobp.2014.09.025>.
- [27] Van Herk M, Remeijer P, Lebesque JV. Inclusion of geometric uncertainties in treatment plan evaluation. *Int J Radiat Oncol Biol Phys* 2002;52:1407–22. [https://doi.org/10.1016/S0360-3016\(01\)02805-x](https://doi.org/10.1016/S0360-3016(01)02805-x).
- [28] Witte MG, Sonke J, Siebers J, et al. Beyond the margin recipe: the probability of correct target dosage and tumor control in the presence of a dose limiting structure. *Phys Med Biol* 2017;62:7874–88. <https://doi.org/10.1088/1361-6560/aa87fe>.
- [29] Shimomura A, Wu T, Rusu I, et al. Monitoring intrafraction motion of the prostate during radiation therapy: suggested practice points from a focused review. *Pract Radiat Oncol* 2024;14:146–53. <https://doi.org/10.1016/j.prro.2023.08.017>.
- [30] Pathmanathan AU, McNair HA, Schmidt MA, et al. Comparison of prostate delineation on multimodality imaging for MR-guided radiotherapy. *Br J Radiol* 2019;92. <https://doi.org/10.1259/bjr.20180948>.
- [31] Gibson E, Bauman GS, Romagnoli C, et al. Toward prostate cancer contouring guidelines on magnetic resonance imaging: Dominant lesion gross and clinical target volume coverage via accurate histology fusion. *Int J Radiat Oncol Biol Phys* 2016;96:188–96. <https://doi.org/10.1016/j.ijrobp.2016.04.018>.
- [32] Van Houdt PJ, Ghobadi G, Schoots IG, et al. Histopathological features of MRI-invisible regions of prostate cancer lesions. *J Magn Reson Imaging* 2020;51:1235–46. <https://doi.org/10.1002/jmri.26933>.
- [33] Kramer M, Sphon SK, Kiefer S, et al. Isotropic expansion of the intraprostatic gross tumor volume of primary prostate cancer patients defined in MRI – a correlation study with whole mount histopathological information as reference. *Front Oncol* 2020;10. <https://doi.org/10.3389/fonc.2020.596756>.
- [34] Grefve J, Söderkvist K, Gunnlaugsson A, et al. Histopathology-validated gross tumor volume delineations of intraprostatic lesions using PSMA-positron emission tomography/multiparametric magnetic resonance imaging. *Phys Imag Radiat Oncol* 2024. <https://doi.org/10.1016/j.phro.2024.100633>.
- [35] Steenbergen P, Hausermans K, Lerut E, et al. Prostate tumor delineation using multiparametric magnetic resonance imaging: inter-observer variability and pathology validation. *Radiother Oncol* 2015;115:186–90. <https://doi.org/10.1016/j.radonc.2015.04.012>.
- [36] Bettermann AS, Zamboglou C, Kiefer S, et al. [68Ga]-PSMA-11 PET/CT and multiparametric MRI for gross tumor volume delineation in a slice by slice analysis with whole mount histopathology as a reference standard – Implications for focal radiotherapy planning in primary prostate cancer. *Radiother Oncol* 2019;141:214–9. <https://doi.org/10.1016/j.radonc.2019.07.005>.
- [37] Menne Guricová K, Draulans C, Pos FJ, et al. Focal boost to the intraprostatic tumor in external beam radiotherapy for patients with localized prostate cancer: 10-year outcomes of the FLAME trial. *J Clin Oncol* 2025;43:3065–9. <https://doi.org/10.1200/JCO-25-00274>.
- [38] De Muinck Keizer DM, Kerkmeijer LG, Willigenburg T, et al. Prostate intra-fraction motion during the preparation and delivery of MR-guided radiotherapy sessions on a 1.5T MR Linac. *Radiother Oncol* 2020;151:88–94. <https://doi.org/10.1016/j.radonc.2020.06.044>.
- [39] Dassen MG, Janssen T, Kusters M, et al. Comparing adaptation strategies in MRI-guided online adaptive radiotherapy for prostate cancer: Implications for treatment margins. *Radiother Oncol* 2023;186. <https://doi.org/10.1016/j.radonc.2023.109761>.
- [40] Wahlstedt I, Andratschke N, Behrens CP, et al. Gating has a negligible impact on dose delivered in MRI-guided online adaptive radiotherapy of prostate cancer. *Radiother Oncol* 2022;170:205–12. <https://doi.org/10.1016/j.radonc.2022.03.013>.
- [41] Janssen TM, Van der Heide UA, et al. A margin recipe for the management of intrafraction target motion in radiotherapy. *Phys Imag Radiat Oncol* 2022;24:159–66. <https://doi.org/10.1016/j.phro.2022.11.008>.
- [42] Neylon J, Ma TM, Savjani R, et al. Quantifying intrafraction motion and the impact of gating for magnetic resonance imaging-guided stereotactic radiation therapy for prostate cancer: analysis of the magnetic resonance imaging arm from the MIRAGE phase 3 randomized trial. *Int J Radiat Oncol Biol Phys* 2024;118:1181–91. <https://doi.org/10.1016/j.ijrobp.2023.12.035>.
- [43] Tsekas G, Zachiu C, Bol GH, et al. Investigating the use of comprehensive motion monitoring for intrafraction 3D drift assessment of hypofractionated prostate cancer patients on a 1.5T magnetic resonance imaging radiotherapy system. *Phys Imag Radiat Oncol* 2024;31. <https://doi.org/10.1016/j.phro.2024.100596>.
- [44] Hearn N, Blazak J, Vivian P, et al. Prostate cancer GTV delineation with biparametric MRI and 68Ga-PSMA-PET: comparison of expert contours and semi-automated models. *Br J Radiol* 2021;94:20201174. <https://doi.org/10.1259/bjr.20201174>.
- [45] Wise AM, Stamey TA, McNeal JE, et al. Morphologic and clinical significance of multifocal prostate cancers in radical prostatectomy specimens. *Adult Urol* 2002;60:264–9. [https://doi.org/10.1016/S0090-4295\(02\)01728-4](https://doi.org/10.1016/S0090-4295(02)01728-4).
- [46] Turkbey B, Mani H, Shah V, et al. Multiparametric 3T prostate magnetic resonance imaging to detect cancer: histopathological correlation using prostatectomy specimens processed in customized magnetic resonance imaging based molds. *J Urol* 2011;186:1818–24. <https://doi.org/10.1016/j.juro.2011.07.013>.
- [47] Le JD, Tan N, Shkolyar E, et al. Multifocality and prostate cancer detection by multiparametric magnetic resonance imaging: correlation with whole-mount histopathology. *Eur Urol* 2015;67:569–76. <https://doi.org/10.1016/j.eururo.2014.08.079>.
- [48] Salembier C, Villeirs G, De Bari B, et al. ESTRO ACROP guideline on CT- and MRI-based target volume delineation for primary radiation therapy of localized prostate cancer. *Radiother Oncol* 2018;127:49–61. <https://doi.org/10.1016/j.radonc.2018.01.014>.
- [49] Menne Guricová K, Pos FJ, Schoots IG, et al. Intra-prostatic recurrences after radiotherapy with focal boost: location and dose mapping in the FLAME trial. *Radiother Oncol* 2024. <https://doi.org/10.1016/j.radonc.2024.110535>.

- [50] Shusharina N, Craft D, Chen Y, et al. The clinical target distribution: a probabilistic alternative to the clinical target volume. *Phys Med Biol* 2018;63. <https://doi.org/10.1088/1361-6560/aacfb4>.
- [51] Buti G, Souris K, Barragán Montero AM, et al. Introducing a probabilistic definition of the target in a robust treatment planning framework. *Phys Med Biol* 2021;66. <https://doi.org/10.1088/1361-6560/ac1265>.
- [52] Ferjancić P, Van der Heide UA, Menard C, et al. Probabilistic target definition and planning in patients with prostate cancer. *Phys Med Biol* 2021;66. <https://doi.org/10.1088/1361-6560/c2f8a>.
- [53] Wang Z, Zhou Z, Wang C, et al. Microscopic spread of low rectal cancer in regions of mesorectum: pathologic assessment with whole-mount sections. *World J Gastroenterol* 2004;10:2949–53. <https://doi.org/10.3748/wjg.v10.i20.2949>.
- [54] Kerkmeijer LG, Groen VH, Pos FJ, et al. Focal boost to the intraprostatic tumor in external beam radiotherapy for patients with localized prostate cancer: results of the FLAME randomized phase III trial. *J Clin Oncol* 2021;39:787–96. <https://doi.org/10.1200/JCO.20.02873>.